

**Nondivergent spinning substructures near acoustic field nodes**Andrew Kille  and Andrei Afanasev <sup>\*</sup>*Department of Physics, George Washington University, Washington, District of Columbia 20052, USA*

(Received 9 January 2024; revised 2 April 2024; accepted 26 April 2024; published 7 May 2024)

In this work, we examine the extraordinary behavior of polarization and spin angular momentum density in the vicinity of longitudinal field zeros in three-dimensional monochromatic acoustic fields. We demonstrate that, as governed by the continuity equation, the velocity fields of arbitrary acoustic sources maintain nondiffractive elliptical polarization structures that enclose longitudinal field zeros, despite having divergent transverse spatial profiles of intensity. Furthermore, embedded in these nonparaxial field contours, for infinite distance, are threads of circular polarization singularities. We illuminate these inherent properties in acoustic vortex fields, dipole arrays, and the famous Young's double-slit experiment. Our results reveal spin characteristics of sound waves that provide a platform for future studies and applications of structured acoustic waves and chiral acoustic phenomena.

DOI: [10.1103/PhysRevB.109.184305](https://doi.org/10.1103/PhysRevB.109.184305)**I. INTRODUCTION**

Singularities in complex inhomogeneous scalar and vector wave fields exhibit rich topological characteristics. In classical vector waves, there exists a fundamental property known as polarization, in which an abundance of singular features has been studied extensively, particularly those features found in structured monochromatic light [1,2]. Structured acoustic waves with twisted wave fronts carrying orbital angular momentum were first demonstrated experimentally in Ref. [3]. Recent theoretical and experimental results demonstrate analogous properties of polarization and angular momenta in the longitudinal (curl-free) vector velocity fields of acoustic waves [4–9], opening an avenue for future applications in acoustic tweezers [10–13], acoustofluidics [14,15], underwater communications [16,17], and biomedical imaging [18–20].

In paraxial sound, the velocity field vector is approximately collinear with wave vector  $\mathbf{k}$ , yielding a homogeneous distribution of linear polarization in space. This constraint is reasonable for distances far from a localized acoustic source; however, in the near field, all spatial field components are substantial (i.e., nonparaxial in nature). The local rotational field trajectories associated with nonparaxial sound are highly nontrivial [6,21], and can be described by a dynamical variable known as spin angular momentum (SAM) density. Peculiar manifestations of SAM density arise in both optics and acoustics, notably, the signature of transverse spin, for example, in evanescent waves [6,22,23] and two-wave interference [24].

Threads of polarization singularities, such as lines of strictly circular and linear polarization, are imprinted in vector waves due to the natural occurrence of field zeros. It was shown recently [25] that optical vortex beams possess remarkable and nonintuitive features of nondiffractive polarization near the phase singularities for arbitrary large distances.

Moreover, a study found that such polarization and momentum structures exist around any persisting transverse field zero (thread of linear polarization) of electromagnetic radiation and light interference patterns from an arbitrary localized source [26]. Evidently, this general phenomenon of light originates from Maxwell electromagnetism and the stability of electromagnetic nulls in the far field.

In this text, motivated by these studies [25,26], we analyze the general properties of polarization and spin near singular imprints of nonparaxial monochromatic acoustic waves. We show that intrinsic field zeros (phase singularities) produce remarkable nondivergent vector characteristics of sound, in direct analogy with features found in light. Indeed, accompanying polarization structures of invariant and stable cross section formed by the vector velocity fields from a localized acoustic source are persistent lines of polarization singularities. Thus, we reveal vectorial structures universal to all forms of acoustic radiation. To illustrate these results, we consider nonparaxial, diverging acoustic vortex beams, a wavelength-spaced acoustic dipole array, and Young's double-slit interference. This work offers numerous possibilities to experimentally utilize the spin features of acoustic waves.

While we are aware of the studies demonstrating strong nonlinearity near phase singularities of acoustic fields [27], our present approach is linear, since we consider effects in low-intensity regions beyond the near field of interference patterns.

**II. GENERAL THEORY****A. Background**

In this section, we briefly review relevant equations of motion and dynamical properties of acoustic waves. In addition, we discuss acoustic polarization singularities and define a polarization parameter important for analyzing spatial distributions of individual velocity field components.

<sup>\*</sup> [afanas@gwu.edu](mailto:afanas@gwu.edu)

Let us consider monochromatic acoustic waves of frequency  $\omega$  in a homogeneous medium of mass density  $\varrho_0$  and compressibility  $\beta$ :

$$\nabla \cdot \mathbf{V} = i\beta\omega P, \quad \nabla P = i\varrho_0\omega \mathbf{V}, \quad (1)$$

where  $P(\mathbf{r})$  and  $\mathbf{V}(\mathbf{r})$  are the complex scalar pressure and vector velocity fields, respectively. The vector velocity field is longitudinal ( $\nabla \times \mathbf{V} = \mathbf{0}$ ), yet in the nonparaxial regime can be generally written in terms of its transverse and longitudinal components:  $\mathbf{V}(\mathbf{r}) = \mathbf{V}_\perp(\mathbf{r}) + V_\parallel(\mathbf{r})\hat{\mathbf{e}}_\parallel$ , where  $\hat{\mathbf{e}}_\parallel$  denotes the unit vector collinear with  $\mathbf{k}$ . The degree in which  $\mathbf{V}(\mathbf{r})$  is circularly polarized is given by the normalized SAM density,

$$\mathbf{S} = \frac{\text{Im}\{\mathbf{V}^* \times \mathbf{V}\}}{|\mathbf{V}|^2}. \quad (2)$$

In plane acoustic waves, the SAM density vanishes; however, inhomogeneous fields produce nonzero SAM density orthogonal to the polarization ellipse. Moreover, the time-averaged energy density of the acoustic fields is

$$W = \frac{1}{4}(\beta|P|^2 + \varrho_0|\mathbf{V}|^2). \quad (3)$$

Note that the transverse spatial extent of energy density  $W$  naturally diverges with respect to distance from a source, with theoretical exceptions such as Bessel and Airy beams.

In direct analogy to the singular behavior around transverse field zeros of electromagnetic fields, vanishing longitudinal velocity of acoustic waves yields nearby velocity fields that are circularly polarized; i.e., the orientation of the polarization ellipse axes is undefined. Note that lines of circular polarization (commonly referred to as C lines [28,29]) exist where  $\mathbf{V}(\mathbf{r}) \cdot \mathbf{V}(\mathbf{r}) = 0$ , which is equivalent to the spin condition  $|\mathbf{S}(\mathbf{r})| = 1$ .

Here, we use a quantity introduced in [25,26], which we label the ‘‘TL-alignment’’ parameter  $\chi_{\text{TL}}$ :

$$\chi_{\text{TL}} = \frac{|\mathbf{V}_\perp|^2 - |V_\parallel|^2}{|\mathbf{V}|^2}. \quad (4)$$

Note that  $\chi_{\text{TL}}$  provides a concise description of the relative transverse-to-longitudinal (TL) field distributions in space; e.g., it follows from Eq. (4) that for  $V_\parallel = 0$ , we have  $\chi_{\text{TL}} = 1$ ; likewise,  $\mathbf{V}_\perp = \mathbf{0}$  gives  $\chi_{\text{TL}} = -1$ . It was shown in [25,26] for optical vortex beams and general electromagnetic radiation that the contour  $\chi_{\text{TL}} = 0$  draws out a nondiffracting tube enclosing a transverse zero (thread of linear polarization) for arbitrary distance. In Sec. II B, we demonstrate that a similar effect holds; that is, for any physical source of acoustic waves containing longitudinal field zeros there exists the contour  $|\mathbf{V}_\perp|^2 = |V_\parallel|^2$  of invariant elliptical cross section that extends to infinity.

## B. Formalism

Let us consider far-field acoustic radiation from any localized source, in which the scalar pressure field can be expressed in spherical coordinates  $(r, \theta, \varphi)$  in the general form

$$P(\mathbf{r}) = P_0(\theta, \varphi) \frac{e^{ikr}}{r}, \quad (5)$$

where  $P_0(\theta, \varphi)$  is the far-field directivity factor unique to the source geometry. A straightforward derivation from Eq. (1)

gives the arbitrary vector velocity field:

$$\mathbf{V}(\mathbf{r}) = \begin{pmatrix} V_r \\ V_\theta \\ V_\varphi \end{pmatrix} = \begin{pmatrix} V_{r0}(\theta, \varphi) \\ V_{\theta0}(\theta, \varphi)/r \\ V_{\varphi0}(\theta, \varphi)/r \end{pmatrix} \frac{e^{ikr}}{r}, \quad (6)$$

where the angular factors  $V_{r0}$ ,  $V_{\theta0}$ , and  $V_{\varphi0}$  are

$$\begin{pmatrix} V_{r0}(\theta, \varphi) \\ V_{\theta0}(\theta, \varphi) \\ V_{\varphi0}(\theta, \varphi) \end{pmatrix} = (i\varrho_0\omega)^{-1} \begin{pmatrix} P_0(\theta, \varphi) \\ \frac{\partial P_0(\theta, \varphi)}{\partial \theta} \\ \frac{1}{\sin \theta} \frac{\partial P_0(\theta, \varphi)}{\partial \varphi} \end{pmatrix}. \quad (7)$$

Importantly, the radial component  $V_r$  has  $1/r$  dependence, while the transverse components  $V_\theta$  and  $V_\varphi$  have  $1/r^2$  dependence. Albeit,  $V_r$  dominates in the far field; however when  $V_{r0} = 0$  (i.e.,  $P_0 = 0$ ), the transverse components are non-negligible, enabling nonparaxial polarization near longitudinal velocity nulls. Here, for arbitrary acoustic radiation, the contour  $\chi_{\text{TL}} = 0$  is equivalent to the relation

$$|V_r(\mathbf{r})|^2 = |\mathbf{V}_\perp(\mathbf{r})|^2, \quad (8)$$

where  $|\mathbf{V}_\perp|^2 = \mathbf{V}_\perp^* \cdot \mathbf{V}_\perp = |V_\theta|^2 + |V_\varphi|^2$ . Let us examine the behavior of the left-hand side of Eq. (8), specifically near an angular position  $(\theta_0, \varphi_0)$  such that  $V_{r0}(\theta_0, \varphi_0) = 0$ . Decomposing  $V_r$  into its real and imaginary parts  $\mathbf{V}_r = (\text{Re } V_r, \text{Im } V_r)^T$ , a first-order Taylor expansion in the vicinity of  $(\theta_0, \varphi_0)$  gives linear behavior  $\mathbf{V}_r \simeq \tilde{\mathbf{V}}_r = \mathbf{J}_V \mathbf{u}$ ; that is, we can express the approximate longitudinal component  $\tilde{\mathbf{V}}_r$  in terms of its Jacobian:

$$\mathbf{J}_V = \begin{pmatrix} \text{Re} \frac{\partial V_{r0}}{\partial \theta} & \text{Re} \frac{\partial V_{r0}}{\partial \varphi} \\ \text{Im} \frac{\partial V_{r0}}{\partial \theta} & \text{Im} \frac{\partial V_{r0}}{\partial \varphi} \end{pmatrix} \frac{e^{ikr}}{r} = \mathbf{J}_0 \frac{e^{ikr}}{r}. \quad (9)$$

Note that  $\mathbf{u} = (\theta - \theta_0, \varphi - \varphi_0)^T$  represents the rotated angular space centered around  $(\theta_0, \varphi_0)$ . The Jacobian  $\mathbf{J}_0$  gives a compact, topological description of the dominant longitudinal velocity field near its first-order zeros [i.e., angular positions  $(\theta_0, \varphi_0)$  where  $\det(\mathbf{J}_0) \neq 0$ ] [30]. Now, Eq. (8) can be recast in matrix form, dropping radial factors, as

$$\mathbf{u}^T (\mathbf{J}_0^T \mathbf{J}_0) \mathbf{u} = \frac{1}{r^2} |\mathbf{V}_{\perp 0}|^2, \quad (10)$$

where  $|\mathbf{V}_{\perp 0}|^2 = |V_{\theta 0}|^2 + |V_{\varphi 0}|^2$  is approximately a nonzero constant crossing  $(\theta_0, \varphi_0)$ , with the condition that  $V_r(\theta_0, \varphi_0)$  is a first-order zero. Thus, Eq. (10) satisfies the criterion of an ellipse enclosing  $(\theta_0, \varphi_0)$ , whose cross section scales directly with  $1/r^2$ , thereby exhibiting nondiffractive behavior with respect to radial distance. Geometric properties of the TL-alignment ellipse, which traces out a nondivergent tube for infinite distance, can be derived from Eq. (10). Denoting  $\lambda_1, \lambda_2$  as the eigenvalues of the matrix  $\mathbf{J}_0^T \mathbf{J}_0$ , the semiaxis lengths of the ellipse are

$$a = \frac{1}{r} \sqrt{\frac{|\mathbf{V}_{\perp 0}|^2}{\lambda_1}}, \quad b = \frac{1}{r} \sqrt{\frac{|\mathbf{V}_{\perp 0}|^2}{\lambda_2}}. \quad (11)$$

It follows from Eq. (11) that the real-space cross-sectional area of the tube is  $A = \pi \sin \theta |\mathbf{V}_{\perp 0}|^2 / |\det(\mathbf{J}_0)|$ , which is independent of radial source distance  $r$ .

In the far field, due to the dominant longitudinal velocity  $|\mathbf{V}| \simeq |V_r|$ , the C-line condition becomes  $\mathbf{V} \cdot \mathbf{V} \simeq V_r^2 = 0$ .

This condition is equivalent to intersection of the surfaces  $\text{Re}\{\mathbf{V} \cdot \mathbf{V}\} = 0$  and  $\text{Im}\{\mathbf{V} \cdot \mathbf{V}\} = 0$ , which for brevity we label as  $A$  and  $B$ , respectively. Thus, in the location of  $(\theta_0, \varphi_0)$ , surfaces  $A$  and  $B$  are close to each other; however they do not intersect at  $(\theta_0, \varphi_0)$  due to the presence of the small transverse field component  $\mathbf{V}_\perp$ . Since  $\mathbf{V} \cdot \mathbf{V}$  is approximately quadratic in the far field, then  $A$  and  $B$  take the form of either a hyperbola or an ellipse. Thus, with exceptions of additional degrees of symmetry (see Sec. III for an example in vortex beams),  $A$  and  $B$  intersect either 2 or 4 times in the vicinity of  $(\theta_0, \varphi_0)$ . With increasing radial distance, this approximation becomes nearly exact, so a persistent longitudinal field zero will necessarily have nearby parallel C lines in the far field.

We summarize this formalism as follows. Despite the inevitable divergence of acoustic fields in space, near a far-field node with angular position  $(\theta_0, \varphi_0)$  of any physically realizable source of acoustic radiation, there exist (i) the nonparaxial contour  $|\mathbf{V}_\perp| = |V_r|$  that encloses  $(\theta_0, \varphi_0)$  in the form of a nondivergent elliptical tube with respect to radial distance, and (ii) accompanying paired threads of circular polarization singularities.

### III. ACOUSTIC LAGUERRE-GAUSSIAN BEAMS

First, consider nonparaxial vortex beams, which are identifiable by their phase dislocation along the propagation axis and subsequent degree of orbital angular momentum. We construct an acoustic vortex beam by first describing the pressure field with the scalar Laguerre-Gaussian equation in cylindrical coordinates  $\mathbf{r} = (\rho, \varphi, z)$ :

$$P(\mathbf{r}) = A \frac{w_0}{w(z)} \left( \frac{\rho}{w(z)} \right)^{|\ell|} \mathcal{L}_p^\ell \exp\left(-\frac{\rho^2}{w^2(z)}\right) \times \exp\left\{i\left[\ell\varphi + kz + k\frac{\rho^2}{2R(z)} - (|\ell| + 2p + 1)\xi(z)\right]\right\}, \quad (12)$$

where  $A$  is the normalization constant,  $w_0$  is the beam waist at  $z = 0$ ,  $w(z) = w_0\sqrt{1 + (z/z_R)^2}$  is the beam width for all space, where  $z_R = kw_0^2/2$  is the Rayleigh length,  $R(z) = z[1 + (z_R/z)^2]$  is the radius of curvature,  $\xi(z) = \arctan(z/z_R)$  is the Gouy phase, and  $\mathcal{L}_p^\ell$  is the generalized Laguerre polynomial of azimuthal order  $\ell$  and radial order  $p$ . With Eq. (1), we derive the Cartesian velocity field components

$$V_x(\mathbf{r}) = -\frac{iP^{(\text{LG})}}{\varrho_0\omega} \left( \frac{|\ell|}{\rho} e^{-i\varphi} + \rho \cos\varphi \left[ \frac{k}{R(z)} - \frac{2}{w^2(z)} \right] \right), \quad (13)$$

$$V_y(\mathbf{r}) = -\frac{iP^{(\text{LG})}}{\varrho_0\omega} \left( \frac{|\ell|}{\rho} e^{i\varphi} + \rho \sin\varphi \left[ \frac{k}{R(z)} - \frac{2}{w^2(z)} \right] \right), \quad (14)$$

$$V_z(\mathbf{r}) = \frac{P^{(\text{LG})}}{\varrho_0\omega} \left\{ \frac{iw_0^2}{z_R^2 w^2(z)} \left[ z + |\ell|z - \frac{2\rho^2 z}{w^2(z)} \right] + k \left[ 1 + \frac{\rho^2 z_R^2}{z^2 R^2(z)} - \frac{\rho^2}{2zR(z)} - \frac{w_0^2(|\ell| + 2p + 1)}{kz_R w^2(z)} \right] \right\}. \quad (15)$$

Observe that the longitudinal field component  $V_z$  vanishes along the propagation axis, i.e., where  $(x, y) = (0, 0)$ , leaving nonzero transverse polarization that persists for infinite distance. This phenomena is illustrated in Fig. 1(a), where energy density  $W$  is nonzero at the phase singularity beyond the Rayleigh length. The significance of nonzero intensity at the center of a vortex beam is widely studied in optics [31], particularly in light-matter interactions [32,33]. It should be noted that this effect is not found in acoustic Gaussian beams ( $\ell = 0$ ), which do not possess field nodes.

A straightforward analytical calculation [Eq. (2)] shows that for  $\ell \neq 0$ , the normalized SAM density at the center of the vortex beam is strictly longitudinal  $\mathbf{S} = S_z \hat{\mathbf{z}}$ . As shown in Fig. 1(b),  $S_z = \pm 1$  at the vortex center, corresponding to a line of circular polarization, of which chirality is determined by  $\text{sgn}(\ell)$ . It is found that  $S_z$  persists for infinite distance, as presented in Fig. 1(b), where  $|\mathbf{S}|$  plateaus at unity in the vortex center at  $z = 0$  and  $z = 2z_R$ . Due to the circular symmetry of the Laguerre-Gaussian beam, only a single line of circular polarization is present along the vortex node. Equivalent results for SAM density can be derived for acoustic Bessel beams [6], which possess propagation-invariant energy profiles.

Examining the TL-alignment parameter  $\chi_{\text{TL}}$  near the phase singularity,  $\rho \ll w(z)$ , we find that

$$\chi_{\text{TL}} \simeq \frac{2\xi^2 - 1}{2\xi^2 + 1}, \quad (16)$$

where  $\xi = \ell/(k\rho)$ . As shown in Fig. 1(c), the bounds for  $\chi_{\text{TL}}$  are  $-1 \leq \chi_{\text{TL}} \leq 1$ . The contour  $\chi_{\text{TL}} = 0$  for any acoustic vortex beam of azimuthal order  $\ell$  traces out a cylinder of fixed radius  $\ell\lambda/(\sqrt{2}\pi)$  that encloses the vortex phase singularity for infinite distance, despite an expanding transverse intensity profile [see Fig. 1(a)].

These nondiffractive features survive in the far field for velocity fields of local coaxial and non-coaxial superpositions of monochromatic acoustic Laguerre-Gaussian beams, that is,  $\mathbf{V}(\mathbf{r}) = \sum_i \mathbf{V}_{\ell_i, p_i}(\mathbf{r}_i)$ . Indeed, when  $z \gg D$ , where  $D$  is the size of the source, the superimposed field components near a persisting longitudinal field zero give quadratic behavior akin to Eq. (16). Therefore, regardless of the localized source geometry and mixing of radial and azimuthal orders of acoustic vortex beams, there always exists nondiffractive features in distances sufficiently far from the source. We illustrate this phenomenon in Figs. 1(d)–1(f), which contain intensity and polarization distributions for the non-coaxial superposition of two acoustic vortex beams launched at  $(x, y) = (\pm 1.5\lambda, 0)$ . Around the longitudinal node propagating at  $(x, y) = (0, 0)$ , there exists a pair of C lines that maintain separation of  $\lambda/\pi$  [Fig. 1(e)]. Furthermore, as evident in Fig. 1(f), interference of the individual fields results in a far-field nondiverging TL-alignment tube centered around the origin.

### IV. ACOUSTIC DIPOLE ARRAY

Elaborate zero patterns in acoustics can be created via superposition of fields from multiple acoustic radiators. It follows that rich nondiffracting polarization and spin distributions can be tailored with acoustic arrays. Here, we examine the superimposed acoustic fields from an array of acoustic dipoles, that is,  $P = \sum_i P^{\text{dip}}(\mathbf{r}_i)$  and  $\mathbf{V} = \sum_i \mathbf{V}^{\text{dip}}(\mathbf{r}_i)$ , where

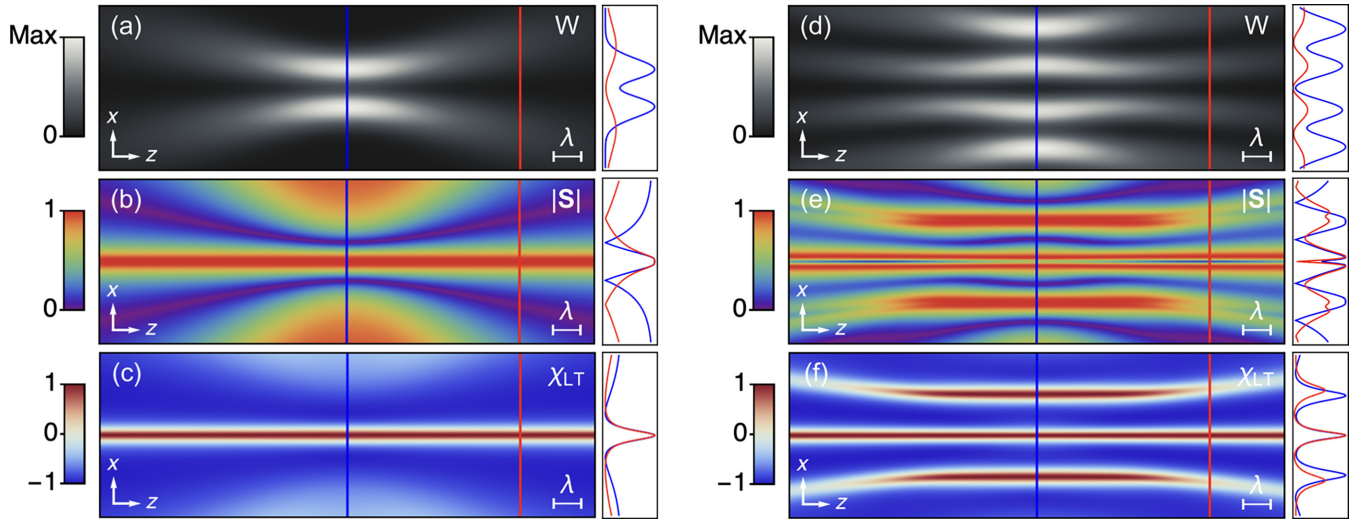


FIG. 1. (a)–(c) Energy density  $W$ , normalized spin AM density  $|S|$ , and TL-alignment parameter  $\chi_{TL}$  for an acoustic Laguerre-Gaussian beam with beam waist  $w_0 = \lambda$  and orders  $\ell = 1, p = 0$  propagating in the  $\hat{z}$  direction. (d)–(f) show the same quantities for non-coaxial superposition of two Laguerre-Gaussian beams ( $\ell = 1, p = 0$ ), each of beam waist  $w_0 = \lambda$ , with spacing  $3\lambda$  along the  $\hat{x}$  axis between their respective centers. In boxes for (a)–(f) are the amplitudes of the corresponding color-density plots at  $z = 0$  (blue) and  $z = 2z_R$  (red).

$P^{\text{dip}}(\mathbf{r}_i)$  and  $\mathbf{V}^{\text{dip}}(\mathbf{r}_i)$  are the pressure and velocity fields, respectively, of the  $i$ th acoustic dipole placed at spatial position  $\mathbf{r}_i$ . Beyond the near field, the angular array factor  $A(\theta, \varphi)$  can be decomposed from  $P$  and  $\mathbf{V}$ , which gives the angular positions  $(\theta_0, \varphi_0)$  of persisting field zeros. It follows that the array geometry, described by  $A(\theta, \varphi)$ , determines angular placement of the nondiffracting structures outlined in the formalism in Sec. II B.

Consider the pressure field of a dipole with moment  $\mathbf{D}$ , which can be expressed in the form [34]

$$P^{\text{dip}}(\mathbf{r}) = -\frac{i}{k} \mathbf{D} \cdot \nabla \left( \frac{e^{ikr}}{kr} \right). \quad (17)$$

Note that the zeros of Eq. (17) occur in the plane orthogonal to  $\mathbf{D}$ . Thus, for a single dipole, there exist degenerate spin structures that enclose the plane where  $P = 0$ . For example, when  $\mathbf{D} = D\hat{z}$ , a Taylor expansion around  $\theta = \pi/2$  of the velocity components  $\mathbf{V}^{\text{dip}} = (V_r, V_\theta, V_\varphi)^T$ , which can be derived from Eq. (1), gives the nondivergent contour  $kr(\theta - \pi/2) = 1$ , independent of azimuthal coordinate  $\varphi$ . Note that  $r_{\parallel} = r(\theta - \pi/2)$  represents the longitudinal distance above the  $z = 0$  plane, so separation of the enclosing contour planes  $\chi_{TL} = 0$  in this case is  $2r_{\parallel} = \lambda/\pi$ .

As an example, we consider a pentagonal array of  $\hat{z}$ -directed acoustic dipoles distributed over a circle of radius  $3\lambda$  in the  $z = 0$  plane [see Fig. 2(a) for a schematic diagram]. Importantly, we do not neglect the transverse components  $\mathbf{V}_{\perp} = (V_\theta, V_\varphi)^T$  of  $\mathbf{V}$ , for their relative size is appreciable near the zeros of  $V_r$ , which enables a nonparaxial description of the velocity fields at certain angular positions in space. As evident in Figs. 2(b) and 2(c), the transverse energy density  $W$  spreads in space with increasing distance  $z$  from the array. Around each propagating dark spot of intensity, we have pairs of C lines which maintain invariant separation of  $\lambda/\pi$  with respect to radial distance. Moreover, enclosing each field node is the nondivergent elliptical tube expressed by the relation

$|\mathbf{V}_{\perp}| = |V_r|$ . This given example demonstrates that nontrivial vectorial information can be embedded in acoustic array fields in a variety of topologies. Our analysis can readily be extended to phased arrays of acoustic antennas, which have wide applicability ranging from biomedical imaging to acoustic microscopy.

## V. DOUBLE-SLIT INTERFERENCE

Our last example is the acoustic version of the famous Young's double-slit experiment of light interference, which was performed in 1801 and subsequently opened a new avenue for the study of wave optics. We provide a standard theoretical analysis of the experiment, with the inclusion of the 3D velocity field components typically neglected due to the curl-free behavior of sound. It follows that nondivergent pairs of circular polarization singularities sandwich the intensity minima (or dark fringes) of the double-slit interference pattern.

As depicted in Fig. 3(a), the experimental geometry is as follows. Consider a screen that consists of two narrow slits, both oriented in the  $\hat{y}$  direction, with spacing  $a$  in the  $\hat{x}$  direction. A projection screen (parallel to the  $xy$  plane) is placed a distance  $z$  from the slits. In the  $y = 0$  plane, the velocity field at a position  $x$  on the projection screen can be expressed as the superposition of monochromatic point sources from each slit:

$$\mathbf{V}^{\text{int}}(\mathbf{r}) = \mathbf{V}_{10} \frac{e^{ikr_1}}{r_1} + \mathbf{V}_{20} \frac{e^{ikr_2}}{r_2}, \quad (18)$$

where  $r_{1,2}$  represents the distance between each slit and the screen measurement position, and  $\mathbf{V}_{10,20} = V_0(\sin \theta_{1,2}, 0, \cos \theta_{1,2})^T \simeq V_0(\theta_{1,2}, 0, 1)^T$  in the Cartesian basis, with the condition  $z \gg x, a$ . The path difference  $r_2 - r_1 = 2\pi m/k$ , where  $m$  is an integer, indicates constructive interference and a bright fringe; likewise, destructive interference occurs at  $r_2 - r_1 = \pi(2m + 1)/k$ , where the dark fringe forms. It follows that the intensity maxima and minima,

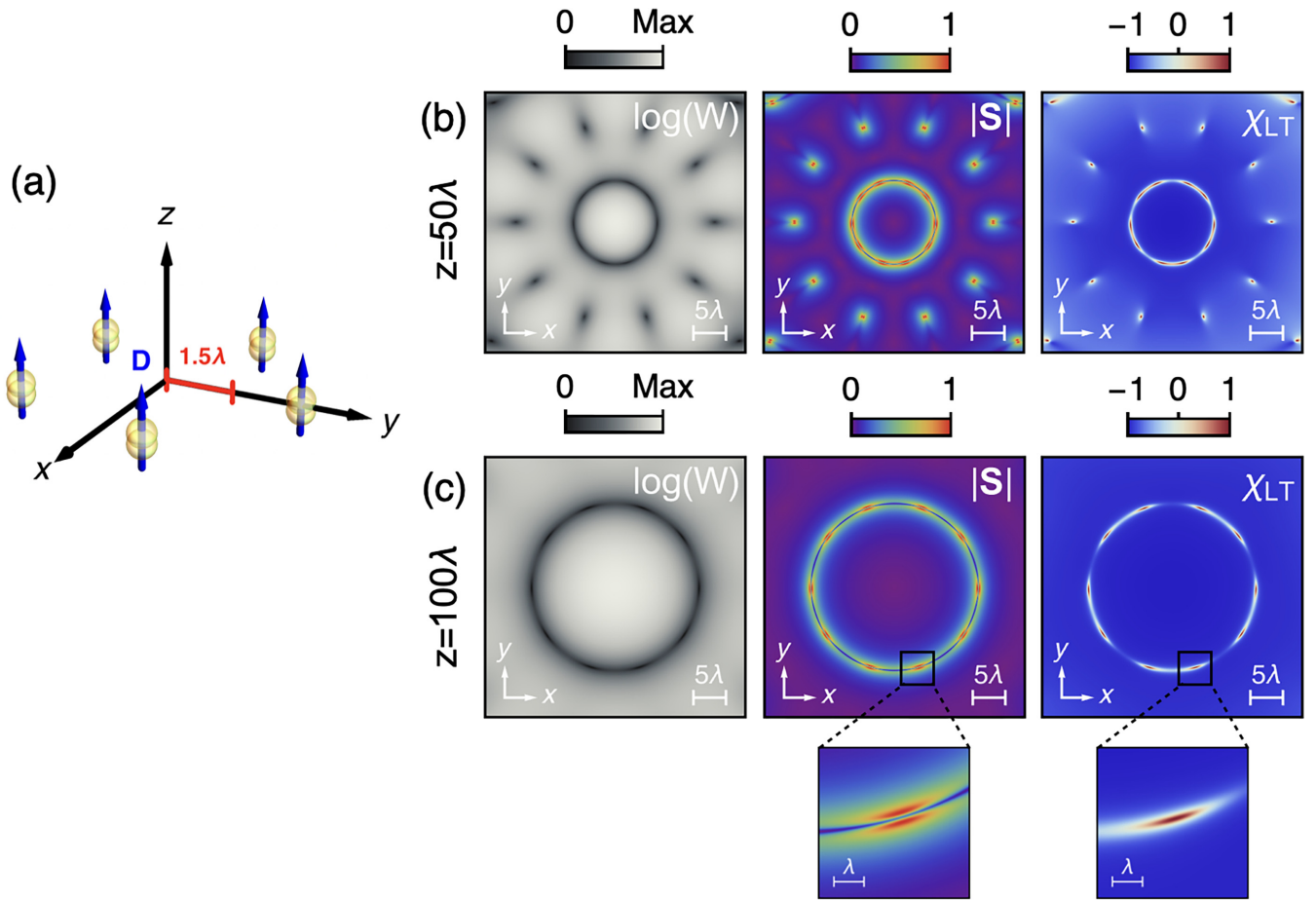


FIG. 2. (a) Schematic diagram of wavelength-spaced dipoles, each with moment  $\mathbf{D} = D\hat{\mathbf{z}}$ , arranged in a pentagonal geometry centered around  $(x, y) = (0, 0)$  in the  $z = 0$  plane. (b) Density plots of logarithmic energy density  $\log(W)$ , normalized SAM density  $|S|$ , and TL-alignment parameter  $\chi_{TL}$  for the superimposed fields directly above the dipole array at  $z = 50\lambda$ . In (c), the same quantities are shown at  $z = 100\lambda$ . Insets for  $|S|$  and  $\chi_{TL}$  are shown around a propagating zero at  $z = 100\lambda$ .

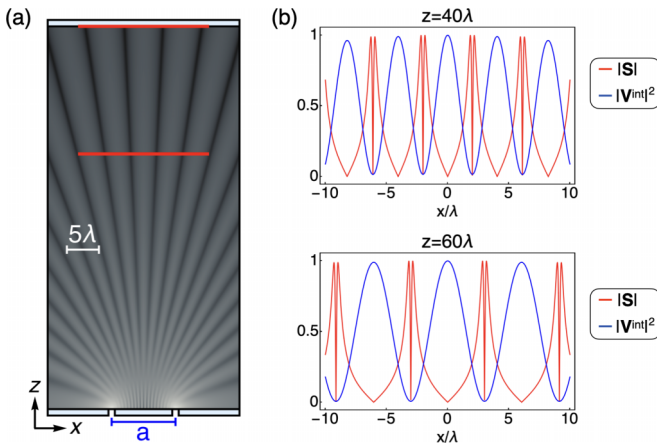


FIG. 3. (a) Sketch of the double-slit interference geometry. The grayscale distribution represents the logarithmic intensity of  $|V^{\text{int}}|$ . (b) Amplitude plots of SAM density  $|S|$  (red) and normalized intensity  $|V^{\text{int}}|^2$  (blue) at  $z = 40\lambda$  and  $z = 60\lambda$ , whose spatial positions with respect to the slits are indicated by the red lines in (a). Pairs of circular polarization singularities or C lines ( $|S| = 1$  corresponding to  $S_y = \pm 1$ ) separated by  $\lambda/\pi$  along  $\hat{\mathbf{x}}$  direction sandwich each intensity minimum at angle  $\alpha_{\min}$  in the far-field zone. Angular positions of C lines are offset by  $\delta\alpha = \pm 1/zk$  with respect to  $\alpha_{\min}$ .

respectively, occur at the angles  $\alpha_{\max} \equiv x_{\max}/z = \lambda m/a$  and  $\alpha_{\min} \equiv x_{\min}/z = \lambda(2m+1)/(2a)$ . For large distances from the slit screen, the longitudinal velocity field component  $V_z^{\text{int}}$  is dominant in comparison to the transverse  $V_x^{\text{int}}$ ; however, evaluating  $V^{\text{int}}$  near  $\alpha_{\min}$  results in comparable spatial field components. Noting that the angular position of each slit occurs at  $\alpha_{1,2} = (x \mp a/2)/z$ , the ratio of velocity field components is derived to be

$$\frac{V_x^{\text{int}}}{V_z^{\text{int}}} = \frac{x}{z} + \frac{a}{2z} \frac{1 - e^{ik(r_1-r_2)}}{1 + e^{ik(r_1-r_2)}}. \quad (19)$$

In the vicinity of  $x_{\min}$ , i.e., locations where  $V_z^{\text{int}} = 0$ , the Taylor expansion  $e^{ik(r_1-r_2)} \simeq -1 + ik\delta r$  results in  $V_x^{\text{int}}/V_z^{\text{int}} \rightarrow \pm i\infty$  as  $\delta r = r_1 - r_2 \rightarrow \mp 0$ , so  $V_z^{\text{int}}$  is a first-order zero at  $x_{\min}$ . Moreover, the complex ratio  $V_x^{\text{int}}/V_z^{\text{int}} = \mp i$ , which satisfies the full circular polarization condition  $S_y = \pm 1$ , occurs when  $x_{\min}$  is offset by  $\delta x = \pm 1/k = \pm \lambda/2\pi$ , independently of the distance between the slits' plane and the projection screen, corresponding to the path difference  $\delta r = \pm a/(zk)$ . Angular offset of the lines with  $S_y = \pm 1$  from the dark fringe position is  $\delta\alpha = \pm 1/zk$ . That is, in the interference pattern emanating from the double slits, we have pairs of circular polarization singularities (C lines) of opposite spins that

maintain a propagation-invariant separation of  $\lambda/\pi$  along the  $x$  axis across each propagating dark fringe of intensity. As demonstrated in Fig. 3(b), within the *intermediate field*, the normalized spin  $|\mathbf{S}|$  rapidly approaches unity where the intensity  $|\mathbf{V}^{\text{int}}|^2$  diminishes, thereby offering a straightforward means to experimentally observe the predicted nondivergent phenomena outside of intensity minima.

We notice an important difference from electromagnetism [26]: While for electromagnetic double-slit interference the spinning structures do not form for field polarization aligned with the slits, there is no such restriction for the longitudinal acoustic pressure waves.

## VI. SUMMARY AND CONCLUSIONS

We have presented a theoretical formalism that predicts nondiffractive polarization and spin structures inherent to acoustic fields of arbitrary sources. The far-field patterns of acoustic radiation yield dominant longitudinal velocity fields due to the curl-free nature of sound; however, near longitudinal zeros (i.e., pressure phase singularities) there exists a rich and invariant nonparaxial region that extends to infinity. In general, accompanying each acoustic field node are the following: a nondivergent elliptical tube whose contour is defined by equality of the longitudinal and transverse velocity fields, and pairs of circular polarization singularities with constant subwavelength separation. The developed formalism can be extended to elastic waves in solids that would also involve shear waves known to lead to polarization anomalies [35,36]. The next step in our studies may be an analysis of surface acoustic waves, for which the polarization singularities predicted here could result in rotation of the velocity field plane near dark fringes of interference.

It is worth comparing our results to those found in electromagnetic fields [25,26]. Despite the contrasting transverse behavior of electric  $\mathbf{E}$  and magnetic  $\mathbf{H}$  fields ( $\nabla \cdot \mathbf{E} = \nabla \cdot \mathbf{H} = 0$ ), it was shown that their transverse field zeros

generate spinning structures analogous to our present work in acoustics. Thus, our findings offer fruitful analogies between light and sound, in regard to the interplay of longitudinal and transverse fields near dark spots of intensity. Furthermore, we have demonstrated that nontrivial elliptical polarization is inherent to all acoustic radiation, despite its curl-free nature.

Due to their occurrence in low-intensity regions, the nondiffracting polarization and spin structures in acoustics require sensitive experimental methods of extracting the nonparaxial velocity fields. This can be accomplished via direct measurement of individual velocity field components with an acoustic vector sensor scanned over 3D space near a field zero, as experimentally demonstrated in Refs. [9,37]. Although acoustic nondiffracting polarization extends infinitely into the far field, a practical experiment will utilize these nonparaxial effects in the intermediate zone and extend to the far-field region, as allowed by the detector's sensitivity. A challenge will be to resolve such vector features for extreme distances from an acoustic source, where the standard measurement device sensitivity is insufficient for such low energy densities. We illustrated our general theory with acoustic vortex beams, acoustic dipole arrays, and Young's double-slit interference, which possess measurable spin structures that emerge close to the source. Indeed, these examples are promising manifestations of nondiffracting phenomena, which could be used for robust beam alignment, detection of acoustic zeros, and resolution of wavelength-dependent spin structures. We are hopeful this work provides potential applications in polarization-based communications, acoustic enantioseparation, nondestructive evaluation of materials, and acoustic tweezers.

## ACKNOWLEDGMENTS

We wish to acknowledge support from U.S. Army Research Office Award No. W911NF-23-1-0085. A.A. thanks Michael Berry and Konstantin Bliokh for useful discussions.

- 
- [1] M. V. Berry, The singularities of light: Intensity, phase, polarisation, *Light Sci. Appl.* **12**, 238 (2023).
  - [2] M. R. Dennis, K. O'Holleran, and M. J. Padgett, in *Singular Optics: Optical Vortices and Polarization Singularities*, edited by E. Wolf, Progress in Optics, Vol. 53 (Elsevier, Amsterdam, Netherlands, 2009), pp. 293–363.
  - [3] B. T. Hefner and P. L. Marston, An acoustical helicoidal wave transducer with applications for the alignment of ultrasonic and underwater systems, *J. Acoust. Soc. Am.* **106**, 3313 (1999).
  - [4] C. R. Courtney, B. W. Drinkwater, C. E. Demore, S. Cochran, A. Grinenko, and P. D. Wilcox, Dexterous manipulation of microparticles using Bessel-function acoustic pressure fields, *Appl. Phys. Lett.* **102**, 123508 (2013).
  - [5] R. D. Muelas-Hurtado, K. Volke-Sepúlveda, J. L. Ealo, F. Nori, M. A. Alonso, K. Y. Bliokh, and E. Brasselet, Observation of polarization singularities and topological textures in sound waves, *Phys. Rev. Lett.* **129**, 204301 (2022).
  - [6] K. Y. Bliokh and F. Nori, Spin and orbital angular momenta of acoustic beams, *Phys. Rev. B* **99**, 174310 (2019).
  - [7] K. Y. Bliokh, M. A. Alonso, D. Sugic, M. Perrin, F. Nori, and E. Brasselet, Polarization singularities and Möbius strips in sound and water-surface waves, *Phys. Fluids* **33**, 077122 (2021).
  - [8] C. Shi, R. Zhao, Y. Long, S. Yang, Y. Wang, H. Chen, J. Ren, and X. Zhang, Observation of acoustic spin, *Natl. Sci. Rev.* **6**, 707 (2019).
  - [9] H. Ge, X.-Y. Xu, L. Liu, R. Xu, Z.-K. Lin, S.-Y. Yu, M. Bao, J.-H. Jiang, M.-H. Lu, and Y.-F. Chen, Observation of acoustic skyrmions, *Phys. Rev. Lett.* **127**, 144502 (2021).
  - [10] A. Ozcelik, J. Rufo, F. Guo, Y. Gu, P. Li, J. Lata, and T. J. Huang, Acoustic tweezers for the life sciences, *Nat. Methods* **15**, 1021 (2018).
  - [11] M. Baudoin and J.-L. Thomas, Acoustic tweezers for particle and fluid micromanipulation, *Annu. Rev. Fluid Mech.* **52**, 205 (2020).
  - [12] D. Baresch, J.-L. Thomas, and R. Marchiano, Observation of a single-beam gradient force acoustical trap for elastic particles: Acoustical tweezers, *Phys. Rev. Lett.* **116**, 024301 (2016).

- [13] J. Li, A. Crivoi, X. Peng, L. Shen, Y. Pu, Z. Fan, and S. Cummer, Three dimensional acoustic tweezers with vortex streaming, *Commun. Phys.* **4**, 113 (2021).
- [14] Y. Fan, X. Wang, J. Ren, F. Lin, and J. Wu, Recent advances in acoustofluidic separation technology in biology, *Microsyst. Nanoeng.* **8**, 94 (2022).
- [15] J. Friend and L. Y. Yeo, Microscale acoustofluidics: Microfluidics driven via acoustics and ultrasonics, *Rev. Mod. Phys.* **83**, 647 (2011).
- [16] X. Li, Y. Li, Q. Ma, G. Guo, J. Tu, and D. Zhang, Principle and performance of orbital angular momentum communication of acoustic vortex beams based on single-ring transceiver arrays, *J. Appl. Phys.* **127**, 124902 (2020).
- [17] J. Heidemann, M. Stojanovic, and M. Zorzi, Underwater sensor networks: Applications, advances and challenges, *Philos. Trans. R. Soc. A* **370**, 158 (2012).
- [18] A. P. Sarvazyan, M. W. Urban, and J. F. Greenleaf, Acoustic waves in medical imaging and diagnostics, *Ultrasound Med. Biol.* **39**, 1133 (2013).
- [19] B. Orazbayev and R. Fleury, Far-field subwavelength acoustic imaging by deep learning, *Phys. Rev. X* **10**, 031029 (2020).
- [20] J. Rufo, P. Zhang, R. Zhong, L. Lee, and T. Huang, A sound approach to advancing healthcare systems: The future of biomedical acoustics, *Nat. Commun.* **13**, 3459 (2022).
- [21] L. Burns, K. Y. Bliokh, F. Nori, and J. Dressel, Acoustic versus electromagnetic field theory: Scalar, vector, spinor representations and the emergence of acoustic spin, *New J. Phys.* **22**, 053050 (2020).
- [22] J. S. Eismann, L. H. Nicholls, D. J. Roth, M. A. Alonso, M. A. Alonso, P. Banzer, F. J. Rodríguez-Fortuño, A. V. Zayats, F. Nori, and K. Y. Bliokh, Transverse spinning of unpolarized light, *Nat. Photonics* **15**, 156 (2021).
- [23] K. Bliokh, A. Bekshaev, and F. Nori, Extraordinary momentum and spin in evanescent waves, *Nat. Commun.* **5**, 3300 (2014).
- [24] A. Y. Bekshaev, K. Y. Bliokh, and F. Nori, Transverse spin and momentum in two-wave interference, *Phys. Rev. X* **5**, 011039 (2015).
- [25] A. Afanasev, J. Kingsley-Smith, F. J. Rodríguez-Fortuño, and A. V. Zayats, Nondiffractive three-dimensional polarization features of optical vortex beams, *Adv. Photonics Nexus* **2**, 026001 (2023).
- [26] A. J. Vernon, A. Kille, F. J. Rodríguez-Fortuño, and A. Afanasev, Non-diffracting polarization features around far-field zeros of electromagnetic radiation, *Optica* **11**, 120 (2024).
- [27] G. Richard, H. S. Lay, D. Giovannini, S. Cochran, G. C. Spalding, and M. P. Lavery, Twisting waves increase the visibility of nonlinear behaviour, *New J. Phys.* **22**, 063021 (2020).
- [28] M. Berry and M. Dennis, Polarization singularities in isotropic random vector waves, *Proc. R. Soc. Lond. Ser. A* **457**, 141 (2001).
- [29] J. Nye and J. Hajnal, The wave structure of monochromatic electromagnetic radiation, *Proc. R. Soc. Lond. Ser. A* **409**, 21 (1987).
- [30] C. M. Spaegle, M. Tamagnone, S. W. D. Lim, M. Ossiander, M. L. Meretska, and F. Capasso, Topologically protected optical polarization singularities in four-dimensional space, *Sci. Adv.* **9**, eadh0369 (2023).
- [31] K. A. Forbes, D. Green, and G. A. Jones, Relevance of longitudinal fields of paraxial optical vortices, *J. Opt.* **23**, 075401 (2021).
- [32] G. F. Quinteiro, F. Schmidt-Kaler, and C. T. Schmiegelow, Twisted-light-ion interaction: The role of longitudinal fields, *Phys. Rev. Lett.* **119**, 253203 (2017).
- [33] A. Afanasev, C. E. Carlson, and H. Wang, Polarization transfer from the twisted light to an atom, *J. Opt.* **22**, 054001 (2020).
- [34] L. Wei and F. J. Rodríguez-Fortuño, Far-field and near-field directionality in acoustic scattering, *New J. Phys.* **22**, 083016 (2020).
- [35] K. Helbig and M. Schoenberg, Anomalous polarization of elastic waves in transversely isotropic media, *J. Acoust. Soc. Am.* **81**, 1235 (1987).
- [36] H. J. Lee, J.-R. Lee, S. H. Moon, T.-J. Je, E.-c. Jeon, K. Kim, and Y. Y. Kim, Off-centered double-slit metamaterial for elastic wave polarization anomaly, *Sci. Rep.* **7**, 15378 (2017).
- [37] H. Ge, S. Liu, X.-Y. Xu, Z.-W. Long, Y. Tian, X.-P. Liu, M.-H. Lu, and Y.-F. Chen, Spatiotemporal acoustic vortex beams with transverse orbital angular momentum, *Phys. Rev. Lett.* **131**, 014001 (2023).